ACS APPLIED MATERIALS & INTERFACES

Research Article

www.acsami.org

Facile Fabrication of Porous $Ni_xCo_{3-x}O_4$ Nanosheets with Enhanced Electrochemical Performance As Anode Materials for Li-Ion Batteries

Fangcai Zheng,[†] Dequan Zhu,[†,§] and Qianwang Chen*[,†,‡]

[†]Hefei National Laboratory for Physical Science at Microscale, Department of Materials Science & Engineering & Collaborative Innovation Center of Suzhou Nano Science and Technology, University of Science and Technology of China, Hefei 230026, China

[‡]High Magnetic Field Laboratory, Hefei Institutes of Physical Science, Chinese Academy of Sciences, Hefei 230031, China

Supporting Information

ABSTRACT: Herein, we report a novel and facile route for the large-scale fabrication of 2D porous $Ni_xCo_{3-x}O_4$ nanosheets, which involves the thermal decomposition of Ni_xCo_{1-x} hydroxide precursor at 450 °C in air for 2 h. The as-prepared 2D porous $Ni_xCo_{3-x}O_4$ nanosheets exhibit an enhanced lithium storage capacity and excellent cycling stability (1330 mA h g^{-1} at a current density of 100 mA g^{-1} after 50 cycles). More importantly, it can render reversible capacity of 844 mA h g^{-1}, even at a high current density of 500 mA g^{-1} after 200 cycles, indicating its potential applications for high power LIBs. Compared to pure Co_3O_4, the reduction of Co in $Ni_xCo_{3-x}O_4$ is of more significance because of the high cost and toxicity of Co. The improved electrochemical performance is attributed to the 2D structure and large amounts of mesopores within the nanosheets, which can effectively improve structural stability, reduce the diffusion length for lithium ions and electrons, and buffer volume expansion during the Li^+ insertion/extraction processes.

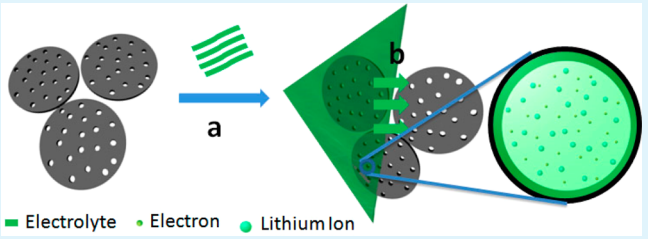

KEYWORDS: *porous nanosheets, binary metal oxides, electrochemical performance, Li-ion batteries*

1. INTRODUCTION

Over the past few years, inspired by the advantages of long lifespan, higher energy density, and environmental benignity, LIBs have been extensively investigated for portable electronic devices and electric vehicles.[1−4] Consequently, a large amount of efforts was made to develop highly efficient, low-cost, and safe electrode candidates for LIBs.[5] Various materials have been designed and prepared as anode materials for LIBs, such as Sn,[6] Si,[7] carbon,[8] and transition metal oxides.[9,10] Commercial graphite electrodes have a theoretical capacity of only 372 mA h g^{-1}, which could not meet the requirements in some application fields. Though Sn and Si anodes deliver higher capacities than graphite anodes, the electrochemical cycling stability is poor due to their significant volume expansion that leads to a dramatic falloff in capacity during cycling.[11,12] Recently, transition-metal oxides with nanostructures have been investigated as anode materials for LIBs because of their high theoretical capacities (500−1000 mA h g^{-1}), short path length of Li^+ diffusion and electron transfer in comparison with their bulk counterparts.[13] For example, transition-metal oxides, such as Co_3O_4,[14] Fe_2O_3,[15] and NiO,[16] have been widely studied as anode materials for LIBs. However, based on previous reports on electrochemical performance of transition-metal oxides, it demonstrates that the best anodic performance is exhibited by Co_3O_4.[17] Chen's group have reported that the capacity value was as high as 1465 mA h g^{-1} and remained stable up to 50 cycles for Co_3O_4 porous nanocages.[18] However, Co_3O_4 is not an ideal electrode candidate in practical applications due to its high cost and toxicity, serious efforts have been made toward replacing Co_3O_4 partially by cheaper and eco-friendly alternative metals. Up to now, preliminary electrochemical performance has been reported on $NiCo_2O_4$ (884 mA h g^{-1}),[19] $CuCo_2O_4$ (755 mA h g^{-1}),[20] $ZnCo_2O_4$ (900 mA h g^{-1}),[21] and $MnCo_2O_4$ (755 mA h g^{-1}),[22] which are all isostructural to Co_3O_4 and show high capacity and stability. Therefore, in recent years, binary transition metal oxides have been considered as promising anode materials for LIBs, because they can efficiently overcome the drawbacks of simple oxides and often integrate two types of functional materials for a synergistic effect that can improve the intrinsic properties of each component including electrochemical reactivity and mechanical stability.[23,24] However, up to now, the cobalt-based sipnel structured binary metal oxides still could not reach the high-level lithium storage capacity of Co_3O_4, which might be attributed to the fact that the suitable structure is not obtained for LIBs. And how to make every atom in nanoparticles beneficial for electrochemical reactions is worthy of consideration. Therefore, it is a great challenge to design and prepare a unique structure that is beneficial for enhanced electrochemical performance for LIBs.

As described above, binary metal oxides have been considered as potential anode materials, which can efficiently contain the electrochemical performance of single metal oxides. Spinel compounds of AB_2X_4 (A, B = metal, X = chalcogen)

Received: March 14, 2014
Accepted: May 22, 2014
Published: May 22, 2014

   dx.doi.org/10.1021/am501512j | ACS Appl. Mater. Interfaces 2014, 6, 9256−9264

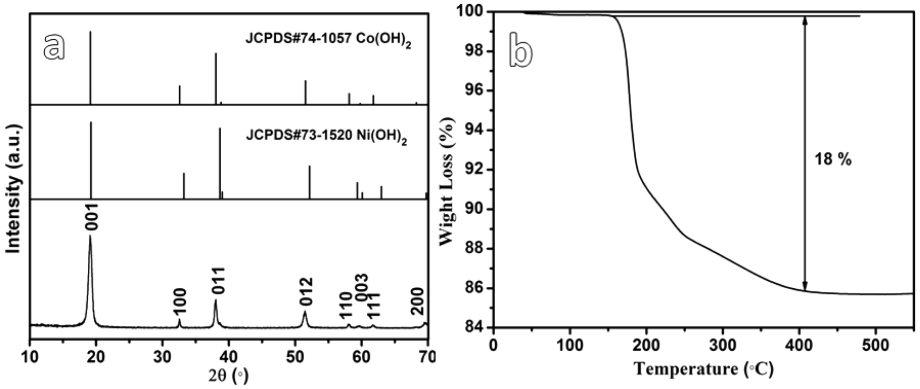

Figure 1. (a) XRD pattern of as-prepared precursor and standard patterns of $Ni(OH)_2$ and $Co(OH)_2$, (b) thermogravimetric analysis (TGA) of as-prepared precursor.

have a large number of superior properties such as low toxicity and low cost, which makes them potentially suitable for anode materials for LIBs.[25,26] As a typical spinel structure, nickel cobaltite ($NiCo_2O_4$), which can be considered as Co in Co_3O_4 partially substituted by Ni, appears to a promising candidate of an anode material for LIBs.[27,28] In comparison with pure NiO and Co_3O_4, it can be believed to be an excellent candidate as an anode material for LIBs due to its notable electrical conductivity and electrochemical activity. Therefore, it deserves to investigate as anode materials for LIBs. In addition to the desirable composition, the electrochemical performance of electrode materials also highly depends on structured feature of the materials. Synthesis of spinel compounds with a distinct structure is significant for the high electrochemical performance of LIBs. Our group has reported that $CoMn_2O_4$ spinel hierarchical microspheres exhibited excellent electrochemical performance for LIBs (894 mA h g^{-1}), which can be attributed to its distinct structure beneficial for enhancing the $CoMn_2O_4$/electrolyte contact area and shortening the Li^+ ion diffusion length during the electrochemical reactions.[29] Porous nanosheets are beneficial for efficient diffusion of the electrolyte and transfer of electrons, which is vital for enhanced electrochemical performance for LIBs. In comparison to cube- and wire-like materials for LIBs, the two-dimensional (2D) textural features, such as sheet-or plate-like, display a huge percentage of surface atoms and specific facet exposed, which makes full use of active materials in the electrode for LIBs. Therefore, it is suggested that spinel structured binary metal oxides with 2D architecture might be superior anode materials for LIBs. However, up to now, the 2D structure of spinel binary metal oxides has rarely been reported for LIBs. Therefore, it is desirable to design and fabricate 2D porous binary metal oxides as anode materials for LIBs, which is favorable for promoting the interface contact area between electrode and electrolyte, facilitating the transfer of lithium ions and electrons and buffering the volume expansion during the charge/discharge processes. At the same time, there are more atoms residing on the surface of 2D architectures, and as a result, the electrode is more active for lithium electrochemical reaction.

In this article, we aim to develop a novel and facile strategy for the large-scale synthesis of 2D Ni_xCo_{1-x} hydroxide precursors, which can be transformed to $Ni_xCo_{3-x}O_4$ nanosheets after the heat treatment in air. During annealing, the release of a large number of gaseous H_2O molecules would generate large surface area and huge pore volume in the nanosheets. The electrochemical performance of as-prepared 2D porous $Ni_xCo_{3-x}O_4$ nanosheets is evaluated as an anode material for LIBs.

2. EXPERIMENTAL SECTION

Materials Preparation. All chemicals were of analytical grade, and were used without any further purification. In a typical procedure, 0.2 mmol of $Ni(AC)_2{\cdot}2H_2O$, 0.4 mmol of $Co(AC){\cdot}2H_2O$, and 0.3 g of L-arginine were added into the mixed solution of 12 mL of deionized water and 6 mL of ethanol to form a transparent pink solution. Then, 1 mL of $NH_3{\cdot}H_2O$ was added into the above solution. After being vigorously for 10 min, the mixture was transferred into a Teflon-lined stainless steel autoclave with a capacity of 25 mL. The autoclave was sealed, maintained at 100 °C for 8 h, and cooled to room temperature. The resulting precipitates were filtered and washed several times with deionized water and absolute ethanol, respectively, and finally dried under oven at 60 °C. After calcining the collected precursor at 450 °C for 2 h with a temperate ramp of 1 °C/min in air, black sipnel metal oxides of $Ni_xCo_{3-x}O_4$ were obtained. The sample was then ready for further characterization.

Material Characterization. The powder X-ray diffraction (XRD) patterns of all samples were recorded with a X-ray diffractometer (Japan Rigaku D/MAX-γA) equipped with Cu−Kα radiation (λ = 1.54178 Å) over the 2θ range of 10−70°. Field emission scanning electron microscopy (FE-SEM) images were collected on a JEOL JSM-6700 M scanning electron microscope. Transmission electron microscopy (TEM) images were taken on Hitachi H-800 transmission electron microscope using an accelerating voltage of 200 kV, and high-resolution transmission electron microscope (HRTEM) (JEOL-2011) was operated at an acceleration voltage of 200 kV. XPS measurements were performed with an ESCALAB 250 X-ray Photoelectron Spectrometer with Al Kα radiation. The Co and Ni content were analyzed by means of an inductively coupled plasma (ICP) spectrometer (Optima 7300 DV). The specific surface area was evaluated at 77 K (Micromeritics ASAP 2020) using the Brunauer−Emmett−Teller (BET) method, whereas the pore volume and pore size were calculated according to the Barrett−Joyner−Halenda (BJH) formula applied to the adsorption branch. Thermogravimetric analysis (TGA) was carried out using a Shimadzu-50 thermoanalyser under air flow.

Electrochemical Measurements. The electrochemical behavior of the porous $Ni_xCo_{3-x}O_4$ nanosheets was examined by using CR2032 coin-type cells with lithium serving as both the counter electrode and the reference electrode. The working electrode was prepared by compressing a mixture of the active materials, conductive material (acetylene black, ATB), and binder (polyvinylidene fluoride (PVDF)) in a weight ratio of $NiCo_2O_4$/carbon/PVDF = 5:3:2 onto a copper foil current collector and then drying at 80 °C for 12 h. The electrolyte used in the cells was 1.00 M $LiPF_6$ in ethylene carbonate and diethyl carbonate (EC:DEC = 1:1). The cells were assembled in an argon-filled glovebox with both the moisture and the oxygen content bellow 1 ppm (Mikrouna, Super (1220/750/900)). The electrode capacity

dx.doi.org/10.1021/am501512j | ACS Appl. Mater. Interfaces 2014, 6, 9256−9264

was measured by a galvanostatic discharge−charge method in the voltage range between 0.01 and 3.0 V on a battery test system (Neware CT-3008W).

3. RESULTS AND DISCUSSION

The 2D porous $Ni_xCo_{3-x}O_4$ nanosheets were controllably synthesized through a facile solvothermal method combined with a simple post annealing process in air. The Ni_xCo_{1-x} hydroxides were first prepared in a mixed solution with an EtOH-H_2O volume ratio of 2. The whole synthesis process is simple without using any surfactant, which is considered to be very facile and suitable for large-scale synthesis. The cobalt and nickel ions are expected to coprecipitate simultaneously in the alkaline condition. In addition, L-arginine containing both $-NH_2$ and $-COOH$ groups can be easily coordinated to metal ions (Ni^{2+} and Co^{2+}) to control the nucleation rate of the precursor. Figure 1a illustrates the XRD pattern of Ni_xCo_{1-x} hydroxide precursor, which is overlapped by $Ni(OH)_2$ (JCPDS card no. 73−1520) and $Co(OH)_2$ (JCPDS card no. 74−1057). Since the designed product can be considered as $Co(OH)_2$ with a small portion of cobalt substituted by nickel, the XRD pattern of the mixed metal hydrate precursor is very similar to that of pure cobalt hydroxide. This phenomenon was also previously reported by other groups.[30] Figure 1b shows the thermogravimetric (TGA) results of Ni_xCo_{1-x} hydroxide precursor. Moreover, according to the TGA results, there is a sharp weight loss between 150 and 400 °C. In order to ensure calcination of the precursor completely, a temperature of 450 °C is chosen as the calcination temperature for the complete conversion of Ni_xCo_{1-x} hydroxide precursor to $Ni_xCo_{3-x}O_4$. As expected, the Ni_xCo_{1-x} hydroxide precursor is thoroughly transformed into $Ni_xCo_{3-x}O_4$ after annealing at 450 °C in air with a heating rate of 1 °C/min. The pattern of the annealing sample, as shown in Figure 2, is similar to the standard patterns

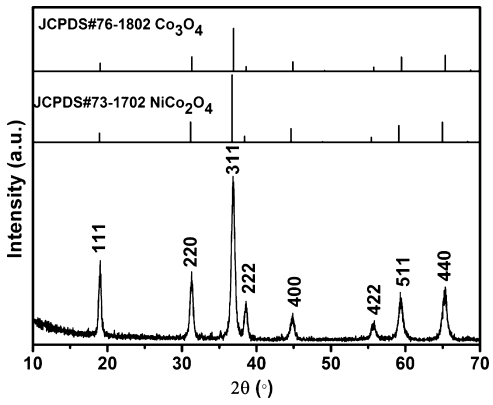

Figure 2. XRD pattern of $Ni_xCo_{3-x}O_4$ obtained by calcining Ni_xCo_{1-x} hydroxide precursor at 450 °C for 2 h in air.

of $NiCo_2O_4$ (JCPDS no. 73−1702) and Co_3O_4 (JCPDS no. 76−1802, suggesting that the mixed nickel cobalt oxide also adopts the spinel structure with similar lattice constants. Quantitative analysis by ICP-AES confirms the Co/Ni atomic ratio of about 4 for the annealing sample. Based on the above analysis, it is reasonably concluded that the nickel cobalt oxide sample synthesized in this work has the chemical composition of $Ni_{0.6}Co_{2.4}O_4$ with a spinel structure.

The size and morphology of the samples were investigated by field-emission scanning electron microscopy (FE-SEM). From the FE-SEM images in Figure 3a,b, it is observed that Ni_xCo_{1-x}

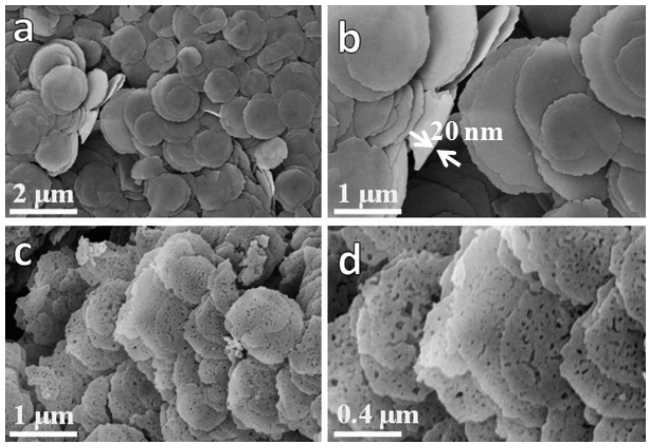

Figure 3. (a, b) SEM images at different magnifications of Ni_xCo_{1-x} hydroxide precursor. (c, d) SEM images at different magnifications of $Ni_xCo_{3-x}O_4$ porous nanosheets.

hydroxide nanosheets are large in scale with about 2 μm in diameter. A typical sheet is about 20 nm thick, which is marked by white arrows in Figure 3b. The $Ni_xCo_{3-x}O_4$ product keeps the original morphology after calcination in air, as shown in Figure 2c,d, indicating the robustness of the structure. At the same time, the surface becomes coarse and porous due to release of gas during the annealing process. To better illustrate the structure and porosity of the as-prepared $Ni_xCo_{3-x}O_4$ product, representative TEM images are shown in Figure 4a,

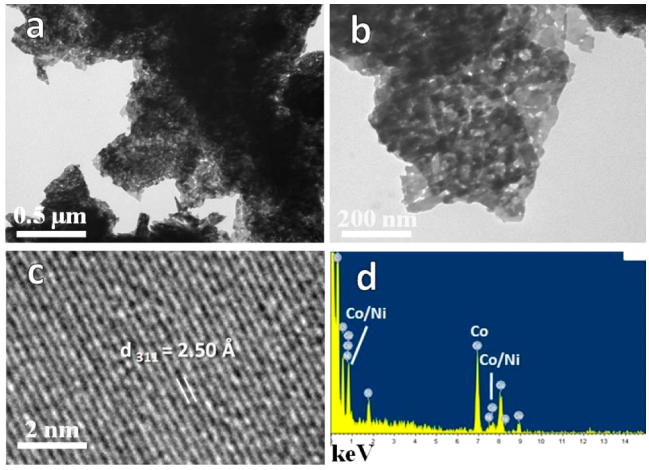

Figure 4. Morphological and elemental analysis of $Ni_xCo_{3-x}O_4$ nanosheets. (a, b) TEM images of $Ni_xCo_{3-x}O_4$ nanosheets. (c) HRTEM of $Ni_xCo_{3-x}O_4$ nanosheets. (d) EDS spectrum of $Ni_xCo_{3-x}O_4$ nanosheets.

b. The as-prepared sample has a 2D porous architecture, and a large number of well-distributed pores can be clearly seen, which is consistent with the result from FE-SEM. A representatively high-resolution TEM (HRTEM) image is shown in Figure 4c, the measured interplanar distance of a randomly selected single nanocrystal is 2.50 Å, which is in good agreement with the (311) plane of spinel $NiCo_2O_4$, thus confirming the XRD analysis. Elemental composition analysis of the $Ni_xCo_{3-x}O_4$ obtained from energy-dispersive X-ray spectroscopy (EDX) indicates the existence of Ni, Co, and O without any other impurity elements (Figure 4d).

dx.doi.org/10.1021/am501512j | ACS Appl. Mater. Interfaces 2014, 6, 9256−9264

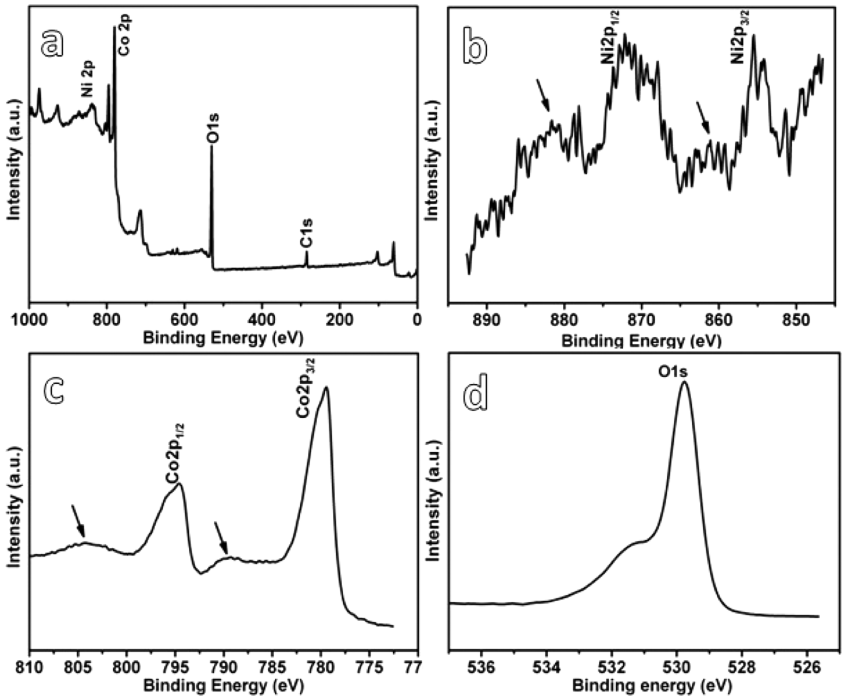

Figure 5. XPS spectra of as-prepared porous $Ni_xCo_{3-x}O_4$: (a) survey spectrum, (b) Ni 2p binding energy spectrum, (c) Co 2p binding energy spectrum, and (d) O 1s binding energy spectrum.

The more detailed elemental composition and oxidation state of as-prepared $Ni_xCo_{3-x}O_4$ annosheets were characterized by X-ray photoelectron (XPS) measurements, the results are shown in Figure 5. The survey spectrum indicates the presence of Co, Ni, O and C in the sample. Figure 5b is the Ni 2p XPS spectrum which shows two major peaks with binding energy at 855.4 and 872.6 eV, corresponding to Ni $2p_{3/2}$ and Ni $2p_{1/2}$, respectively. The arrows in Figure 5b show satellite peaks of Ni $2p_{3/2}$, and Ni $2p_{1/2}$.[27,31] The high-resolution scan of Co 2p of the sample (Figure 5c) exhibits two peaks located at 779.5 and 794.8 eV, which can be assigned to the electronic state of Co $2p_{3/2}$ and Co $2p_{1/2}$, respectively, and the two couple of shakeup satellites.[27] Specifically, the peak at 529.8 eV is typical of metal−oxygen bonds (Figure 5d).[32] No other obvious peaks of impurities were observed. The decomposition of the Ni_xCo_{1-x} hydroxide precursor and the post recrystallization at a relatively low temperature might beneficial for the formation of small metal oxide nanocrystallites. In addition, the gaseous species produced during the calcination process also facilitate to construct the highly porous texture. As a result, abundant pores between the nanoparticles are generated throughout the whole $Ni_xCo_{3-x}O_4$ structures. As we known, the obtained 2D porous structure with a large number of nanopores might be an excellent anode material for LIBs.

The porous texture of the $Ni_xCo_{3-x}O_4$ nanosheets was also investigated at 77 K by the N_2 adsorption−desorption isotherm. As shown in Figure 6, the isotherm profile of the sample can be categorized as a type IV curve with a H3 hysteresis loop at the relative pressure of 0.8−1.0, thus implying the existence of a large number of mesopores in the $Ni_xCo_{3-x}O_4$ sample. From the Barrett−Joyner−Halenda (BJH) pore-size distribution pattern (inset in Figure 6), the above results can be further verified. Additionally, the sample has pore sizes with an average diameter of about 17 nm, which all are in the range of mesopores. Moreover, the Brunauer−Emmett−Teller (BET) surface area is 21.3 $m^2\ g^{-1}$, which is slightly higher than that of

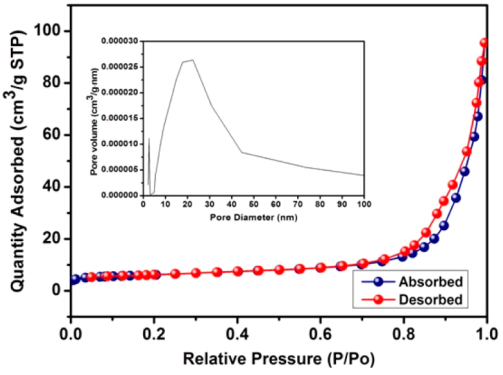

Figure 6. Nitrogen adsorption−desorption isotherm and the corresponding pore size distribution (inset) of $Ni_xCo_{3-x}O_4$ nanosheets.

2D simple metal oxides, such as Mn_2O_3 nanosheets (10.85 $m^2\ g^{-1}$).[33] The mesoporous structure of the $Ni_xCo_{3-x}O_4$ sample may be beneficial for the electrolyte to penetrate completely into the pores and diffuse efficiently to active sites with less resistance, and also can buffers huge volume change during the Li^+ insertion/extraction processes.

The successful fabrication of porous $Ni_xCo_{3-x}O_4$ nanosheets for a superior LIB anode is evident from the extraordinarily excellent electrochemical performance, shown in Figure 7. Figure 7a shows the first three cyclic voltammetry (CV) curves of the electrode made from the porous $Ni_xCo_{3-x}O_4$ nanosheets at room temperature between 0.0 and 3.0 V at a scan rate of 0.1 mV/s. The voltammogram for the first cycle is substantially different from those of the subsequent ones, especially for the discharge branch. In the first cycle, the intense cathodic peak at 0.85 V can be attributed to the reduction of Ni^{3+} or Ni^{2+} and Co^{3+} or Co^{2+} to their metallic states, respectively, whereas the peak at 1.02 V can be assigned to the destruction of the crystal

dx.doi.org/10.1021/am501512j | ACS Appl. Mater. Interfaces 2014, 6, 9256−9264

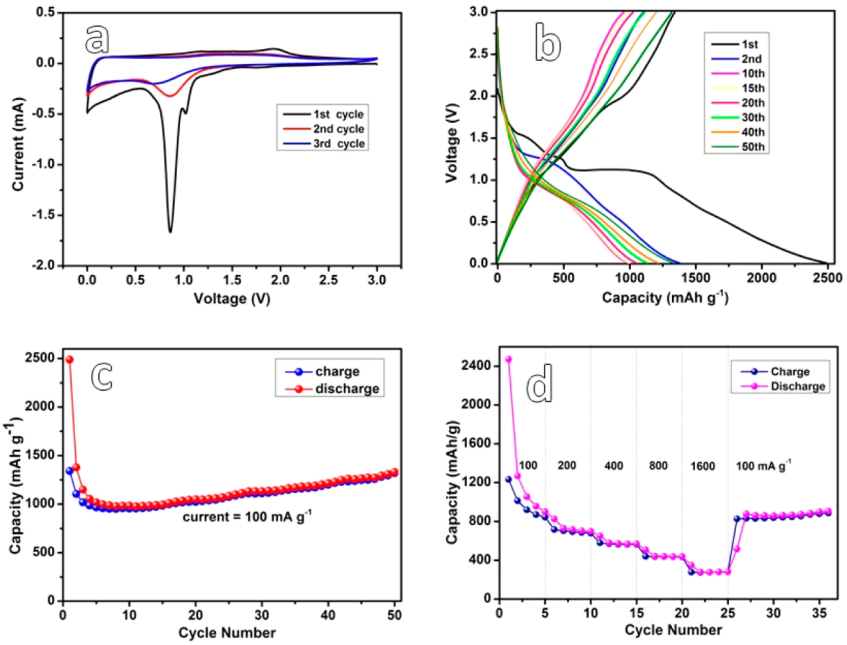

Figure 7. Electrochemical properties of the 2D porous $Ni_xCo_{3-x}O_4$ nanosheets for lithium storage. (a) The first three consecutive CV curves of the electrode made from $Ni_xCo_{3-x}O_4$ nanosheets; (b) discharge−charge curves at a current density of 100 mA g^{-1}; (c) cycling performance of the $Ni_xCo_{3-x}O_4$ nanosheets at a current density of 100 mA g^{-1} in the voltage range 0.01−3.0 vs Li/Li^+; (d) rate capability test for the $Ni_xCo_{3-x}O_4$ nanosheets at various current densities (100−1600 mA g^{-1}).

structure and is easily distinguishable from the other cycles. Additionally, the broad anode peak at about 2.0 V can be assigned to the oxidation of the metallic nickel and cobalt to Ni^{2+} and Co^{2+}, respectively. Apparently, the intensity of the cathodic peak drops significantly in the third cycle relative to that in the second one, indicating the occurrence of some irreversible reactions with the formation of SEI film. Importantly, it is noteworthy that, from the second cycle onward, the CV curves almost overlapped, which indicates the stable and superior reversibility of the sample. On the basis of the CV curves and the above analysis, together with previously reported storage mechanisms for NiO,[34] Co_3O_4,[35] and CoO,[36] the lithium insertion and extraction reactions for our porous $Ni_xCo_{3-x}O_4$ electrode can be expressed as follows

$$Ni_{0.6}Co_{2.4}O_4 + 8Li^+ + 8e^- \rightarrow 0.6Ni + 2.4Co + 4Li_2O \quad (1)$$

$$Ni + Li_2O \leftrightarrow NiO + 2Li^+ + 2e^- \quad (2)$$

$$Co + Li_2O \leftrightarrow CoO + 2Li^+ + 2e^- \quad (3)$$

$$CoO + 1/3Li_2O \leftrightarrow 1/3Co_3O_4 + 2/3Li^+ + 2/3e^- \quad (4)$$

Figure 7b shows representative discharge/charge voltage profiles of the as-prepared sample in different cycles at a current density of 100 mA g^{-1} between 0.01 and 3.0 V. From the profiles, it can be observed that the sample possesses a very high lithium storage capacity of 2489 mA h g^{-1} during the first discharge process, while a relative low reversible capacity of 1340 mA h g^{-1} is achieved, leading to an initial Coulombic efficiency of about 54%. The relative low initial Coulombic efficiency can be attributed to the irreversible capacity loss, including the formation of SEI film and decomposition of electrolyte, which are common to most anode materials.[37,38] This phenomenon also matches well with the CV results that the cathodic peaks are present in the first scan while absent afterward. The discharge voltage plateau at about 1.2 V in the first cycle is different from those of other cycles at about 0.8 V, which further confirms that irreversible reactions occurred in the first cycle. In addition, it is clearly observed that there is a large deviation in potential between charge and discharge curves. This characteristic is commonly exists in a large number of metal oxide anodes, due to the polarization related to ion transfer during cycling processes.[39]

To highlight the superiority of the porous $Ni_xCo_{3-x}O_4$ nanosheets as anode materials for LIBs, we tested the cycle properties of the $Ni_xCo_{3-x}O_4$ electrode at a current density of 100 mA g^{-1} in the range of 0.01−3.0 V vs Li/Li^+. As shown in Figure 7c, the sample displays excellent cycling stability. Moreover, the discharge capacities obtained for the first and second cycles at a current density of 100 mA g^{-1} are 2489 and 1377 mA h g^{-1}, respectively. After tested 10th as an anode electrode for lithium storage, it is interesting to note that the capacities of the sample display a gradual increase during the cycling, which is attributed to the activation of the porous structure. This characteristic is common in a large number of porous materials and cobalt-based materials.[40,41] Therefore, the existence of numerous mesopores in our sample might be beneficial for more electrolyte to gradually access in the porous structure of the electrode materials, which results in the capacity increase during the Li^+ insertion/extraction processes. After 50 cycles at a current density of 100 mA g^{-1}, the discharge capacity is retained at 1330 mA h g^{-1} which is about 96.6% of the second cycle one. This discharge capacity after 50 cycles is about 3.6 times larger than that of the commercial graphite electrode (372 mA h g^{-1}), thereby indicating its high specific capacity. In addition, the porous $Ni_xCo_{3-x}O_4$ sample with 2D architecture exhibits better electrochemical performance than the previous work on $NiCo_2O_4$ as the anode materials for LIBs, such as 884 and 939 mA h g^{-1} at a current density of 89 and 100 mA g^{-1},[42,43] respectively. The electrochemical performance for LIBs is not only superior to the related cobalt-based binary

dx.doi.org/10.1021/am501512j | ACS Appl. Mater. Interfaces 2014, 6, 9256−9264

metal oxides,[19−22] but also approaches to the best capacity of Co_3O_4.[17] To fully understand the electrochemical performance of the as-prepared porous $Ni_xCo_{3-x}O_4$ nanoosheets, we also studied the rate performance of the sample at different rates between 100 and 1600 mA g^{-1} and the charge/discharge curves are shown in Figure 7d. When the current density was gradually increased from 100 to 200, 400, 800, and 1600 mA g^{-1}, the corresponding average discharge capacities were 1331, 736, 589, 454, and 293 mA h g^{-1}, respectively. If the current density was reverted to 100 mA g^{-1} again, the average discharge capacity retained to about 844 mA h g^{-1}, which is a little lower that that obtained at a constant current density of 100 mA g^{-1} (Figure 7c) and has a trend to increase. After charged/discharged at different current densities form 100 to 1600 mA g^{-1}, the cell always cannot show excellent cycling stability as that obtained at a constant current density, which also occur in other materials.[35] This result demonstrates that the porous $Ni_xCo_{3-x}O_4$ nanosheets have great potential as a high-rate anode material for LIBs.

Because the $Ni_xCo_{3-x}O_4$ porous structure presents an outstanding rate capability, the electrochemical performance at a large current density of 500 mA g^{-1} was further evaluated (Figure 8). When a high current density of 500 mA g^{-1} was

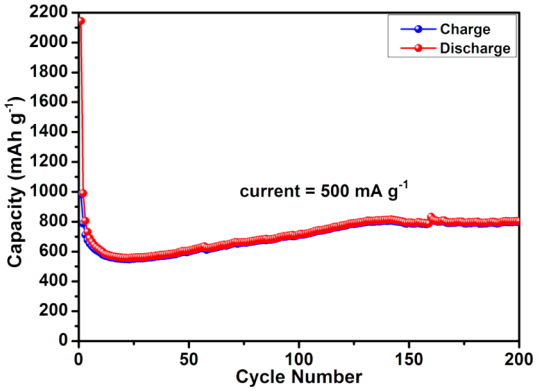

Figure 8. Cycle performance of a $Ni_xCo_{3-x}O_4$ electrode at a current density of 500 mA g^{-1} as a function of cycle number.

directly applied to the cell, the discharge capacity decreased rapidly to 557 mA h g^{-1} after 23 cycles. However, then it slowly increased to 844 mA h g^{-1} after 200 cycles, which is consistent with that carried out at a current density of 100 mA g^{-1}. The result is superior to a latest report in which the $NiCo_2O_4$ has a discharge capacity of 640 mA h g^{-1} after 60 cycles.[43] Importantly, the high-rate discharge/charge is a vital parameter for many practical applications of batteries such as electric vehicles and portable power tools.[44] Additionally, compared to other cobalt-based spinel structure ($ZnCo_2O_4$ microspheres, 721 mAh g^{-1})[45] in which the capacity fades as a function of cycles, the 2D porous $Ni_xCo_{3-x}O_4$ electrodes shows excellent cycling stability as anode materials for LIBs. The unique 2D porous structure of the $Ni_xCo_{3-x}O_4$ sample might be contributed to this excellent electrochemical performance (Scheme 1). On the one hand, the $Ni_xCo_{3-x}O_4$ electrode with 2D architecture is not only beneficial for specific facet exposure, in which lithium insertion is just like surface lithium storage, but also is less prone to structural collapse during cycling processes, which is likely to be the reason why good rate capability and cyclic ability are achieved. Also, these 2D textural features enlarge the interfacial contact area with the electrolyte,

Scheme 1. Schematic Illustration Showing the Diffusion of Electrolyte, Electrons and Lithium Ions[a]

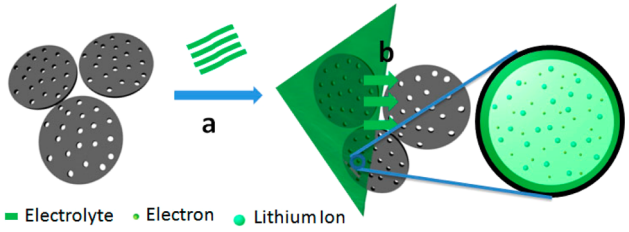

[a](a) The electrolyte can quickly diffuse onto the surface of porous $Ni_xCo_{3-x}O_4$ nanosheets, and further easily diffuse into the inner part of porous $Ni_xCo_{3-x}O_4$ nanosheets from the surface. (b) 2D porous structure can make more atoms residing on the surface, and as a result, the electrode is more active for the lithium electrochemical reaction. Numerous pores store a large number of electrons and lithium ions, which is beneficial for enhanced performance for LIBs.

which shorten the pathway for both lithium ion diffusion and electron transfer. On the other hand, based on previous reports,[46,47] 2D porous nanosheets with an average diameter of 17 nm, especially including mesopores (2−50 nm) and interspacing features,[48] facilitates alleviating the adverse impact of volume expansion during the lithium insertion/extraction processes. Therefore, the 2D porous architecture can provide a carrier for the penetration of the electrolyte and transport of lithium ions and electrons into electrode, and subsequently improve the lithium-storage performance efficiently.

To further investigate the superior electrochemical properties of $Ni_xCo_{3-x}O_4$ nanoporous nanosheets as an anode material, the electrochemical impedance spectra (EIS) of $Ni_xCo_{3-x}O_4$/Li cells at the end of the charge in certain cycles (5th, 15th, 25th) at a current density of 500 mA g^{-1} were measured, which has been proven to be an important and useful tool for evaluating the kinetics of Li insertion electrodes.[49] The semicircle at high frequency can be assigned to the SEI film and contact resistance (R_f), while that at midfrequency is attributed to the charge-transfer impedance on electrode/electrolyte interface (R_{ct}). The linear region corresponds to the semi-infinite diffusion of the lithium ions in the $Ni_xCo_{3-x}O_4$ electrodes (R_e).[50] As clearly shown in Figure 9, the impedance spectra are similar to each other in the shape, with a depressed semicircle in the high and medium frequency regions and a straight line in the low

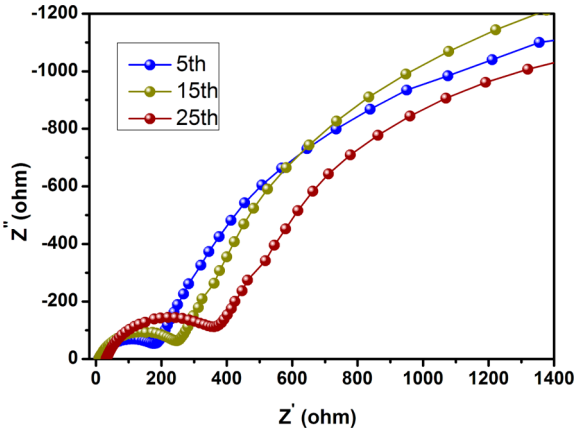

Figure 9. Impedance spectra of $Ni_xCo_{3-x}O_4$ electrode after certain cycles at 500 mA g^{-1} in fully charged state in the frequency range from 10 kHz to 0.1 Hz.

dx.doi.org/10.1021/am501512j | ACS Appl. Mater. Interfaces 2014, 6, 9256−9264

frequency region. Nevertheless, the diameters of the semicircles increase as a function of cycle number, thus indicating the increase of R_f and R_{ct} resistances during the lithium insertion/extraction processes. Based on previous reports,[51] it is a normal phenomenon that occurs in a large number of anode materials. A relatively small decrease in total resistance during cycling was observed, however, the capacities of the sample still displayed a gradual increase. The particles in $Ni_xCo_{3-x}O_4$ nanoporous nanosheets become smaller because of the electrochemical milling during the discharge/charge processes, and therefore the grain boundary increases, which results in an increase in R_{ct} resistance. Meanwhile, the ion conductivity increases with the degradation of the SEI film during cycling,[52,53] which might be one of the vital factors for determining the capacity of LIBs.

For a comparison, Ni_xCo_{1-x} hydroxide precursor was also annealed in air at 400 °C with a temperature ramp of 1 °C/min to obtain another sample of $Ni_xCo_{3-x}O_4$ (see Figure S1 and S2 in the Supporting Information). Its electrochemical performance is not better than that of the $Ni_xCo_{3-x}O_4$ nanosheets synthesized at 450 °C. After 100 cycles at 500 mA g^{-1}, the charge capacity of the $Ni_xCo_{3-x}O_4$ nanosheets obtained at 400 °C is 658 mAh g^{-1} (see Figure S3 in the Supporting Information), whereas the charge capacity of the $Ni_xCo_{3-x}O_4$ nanosheets obtained at 450 °C is 711 mAh g^{-1} (Figure 8). This result demonstrates the effect of calcination temperature for precursor on the electrochemical performance of final material. To verify structural integrity of the $Ni_xCo_{3-x}O_4$ anodes after lithium cycling, batteries were disassembled and examined by SEM and TEM, respectively. Figure S4a,b in the Supporting Information shows the SEM and TEM images of the electrode (obtained at 450 °C) cycled for 20 cycles at a current density of 500 mA g^{-1}, respectively. Unfortunately, the 2D architecture of the $Ni_xCo_{3-x}O_4$ nanosheets is not clearly observed, because the 2D porous architecture is covered by a SEI film and the mixtures of PVDF and acetylene black. Additionally, pores in the 2D porous nanosheets are filled presumably by the residual Li_2O or SEI materials, indicating that pores provide a secondary expansion pathway. This phenomenon demonstrates that the 2D porous nanosheets are ideal candidates for next generation high performance LIBs.

4. CONCLUSIONS

In summary, we have developed a facile and efficient method to prepare uniform 2D mesoporous $Ni_xCo_{3-x}O_4$ nanosheets by decomposition of Ni_xCo_{1-x} hydroxide precursor at a moderate temperature (450 °C) in air. The as-obtained 2D $Ni_xCo_{3-x}O_4$ nanosheets possess high surface area and comprise numerous mesopores. Also, these 2D textural features display a huge percentage of surface atoms and specific facet exposed, which permits a high interfacial contact area with the electrolyte and facilitates electrochemical reactions. Such a unique porous structure not only facilitates the fast transport of lithium ions and electrons but also alleviates the volume expansion during the discharge/charge processes. When tested as an anode material, the $Ni_xCo_{3-x}O_4$ porous nanosheets can retain a reversible capacity of 1330 mA h g^{-1} at 100 mA g^{-1} after 50 cycles, which is about 96.6% of the second cycle one. The reversible capacity approaches to the best one of Co_3O_4. More importantly, its reversible capacity can reach 844 mA h g^{-1} at a relatively high current density of 500 mA g^{-1} after 200 cycles, thus indicating that the porous $Ni_xCo_{3-x}O_4$ nanosheets having a potential as a high-rate anode material for LIBs. In addition, this facile strategy may provide a feasible route for the large-scale fabrication of other 2D porous binary metal oxides which have the potential application in the field of energy storage.

■ ASSOCIATED CONTENT

Supporting Information

XRD, SEM, and TEM patterns of the $Ni_xCo_{3-x}O_4$ nanosheets obtained at 400 °C, cycle performance of the $Ni_xCo_{3-x}O_4$ nanosheets obtained at 400 °C, SEM and TEM images of the electrode. This material is available free of charge via the Internet at http://pubs.acs.org/.

■ AUTHOR INFORMATION

Corresponding Author

*E-mail: cqw@ustc.edu.cn. Fax and Tel: +86 551 63603005.

Notes

The authors declare no competing financial interest.

[§]On leave from Anqing University.

■ ACKNOWLEDGMENTS

This work was supported by the National Natural Science Foundation (NSFC, 21271163, U1232211).

■ REFERENCES

(1) Poizot, P.; Laruelle, S.; Grugeon, S.; Dupont, L.; Tarascon, J.-M. Nano-Sized Transition-Metal Oxides as Negative-Electrode Materials for Lithium-Ion Batteries. *Nature* **2000**, *407*, 496−499.

(2) Ji, L. W.; Lin, Z.; Alcoutlabi, M.; Zhang, X. W. Recent Developments in Nanostructured Anode Materials for Rechargeable Lithium-Ion Batteries. *Energy Environ. Sci.* **2011**, *4*, 2682−2699.

(3) Wang, H. L.; Cui, L. F.; Yang, Y.; Casalongue, H. S.; Robinson, J. T.; Liang, Y. Y.; Cui, Y.; Dai, H. J. Mn_3O_4-Graphene Hybrid as a High-Capacity Anode Material for Lithium Ion Batteries. *J. Am. Chem. Soc.* **2010**, *132*, 13978−13980.

(4) Li, Y. G.; Tan, B.; Wu, Y. Y. Mesoporous Co_3O_4 Nanowire Arrays for Lithium Ion Batteries with High Capacity and Rate Capability. *Nano Lett.* **2008**, *8*, 265−270.

(5) Zhou, L.; Zhao, D. Y.; (David) Lou, X. W. Double-Shelled $CoMn_2O_4$ Hollow Microcubes as High-Capacity Anodes for Lithium-Ion Batteries. *Adv. Mater.* **2012**, *24*, 745−748.

(6) Zhang, W. M.; Hu, J. S.; Guo, Y. G.; Zheng, S. F.; Zhong, L. S.; Song, W. G.; Wan, L. J. Tin-Nanoparticles Encapsulated in Elastic Hollow Carbon Spheres for High-Performance Anode Material in Lithium-Ion Batteries. *Adv. Mater.* **2008**, *20*, 1160−1165.

(7) Zhou, X. S.; Yin, Y. X.; Wan, L. J.; Guo, Y. G. Facile Synthesis of Silicon Nanoparticles Inserted into Graphene Sheets as Improved Anode Materials for Lithium-Ion Batteries. *Chem. Commun.* **2012**, *48*, 2198−2200.

(8) Qie, L.; Chen, W. M.; Wang, Z. H.; Shao, Q. G.; Li, X.; Yuan, L. X.; Hu, X. L.; Zhang, W. X.; Huang, Y. H. Nitrogen-Doped Porous Carbon Nanofiber Webs as Anodes for Lithium Ion Batteries with a Superhigh Capacity and Rate Capability. *Adv. Mater.* **2012**, *24*, 2047−2050.

(9) Chen, J.; Xia, X. H.; Tu, J. P.; Xiong, Q. Q.; Yu, Y. X.; Wang, X. L.; Gu, C. D. Co_3O_4-C Core-Shell Nanowire Array as an Advanced Anode Material for Lithium Ion Batteries. *J. Mater. Chem.* **2012**, *22*, 15056−15061.

(10) Deng, Y. F.; Zhang, Q. M.; Shi, Z. C.; Han, L. J.; Peng, F.; Chen, G. H. Synergies of the Crystallinity and Conductive Agents on the Electrochemical Properties of the Hollow Fe_3O_4 Spheres. *Electrochim. Acta* **2012**, *76*, 495−503.

(11) Nara, H.; Fukuhara, Y.; Takai, A.; Komatsu, M.; Mukaibo, H.; Yamauchi, Y.; Momma, T.; Kuroda, K.; Osaka, T. Cycle and Rate Properties of Mesoporous Tin Anode for Lithium Ion Secondary Batteries. *Chem. Lett.* **2008**, *37*, 142−143.

(12) McDowell, M. T.; Lee, S. W.; Ryu, I.; Wu, H.; Nix, W. D.; Choi, J. W.; Cui, Y. Novel Size and Surface Oxide Effects in Silicon

Nanowires as Lithium Battery Anodes. *Nano Lett.* **2011**, *11*, 4018−4025.
(13) Wang, Z. Y.; Zhou, L.; (David) Lou, X. W. Metal Oxide Hollow Nanostructures for Lithium-ion Batteries. *Adv. Mater.* **2012**, *24*, 1903−1911.
(14) Jayaprakash, N.; Jones, W. D.; Moganty, S. S.; Archer, L. A. Composite Lithium Battery Anodes Based on Carbon@Co_3O_4 Nanostructures: Synthesis and Characterization. *J. Power Sources* **2012**, *200*, 53−58.
(15) Zhang, L.; Wu, H. B.; Xu, R.; (David) Lou, X. W. Porous Fe_2O_3 Nanocubes Derived from MOFs for Highly Reversible Lithium Storage. *CrystEngComm.* **2013**, *15*, 9332−9335.
(16) Mondal, A. K.; Su, D. W.; Wang, Y.; Chen, S. Q.; Wang, G. X. Hydrothermal Synthesis of Nickel Oxide Nanosheets for Lithium-Ion Batteries and Supercapacitors with Excellent Performance. *Chem.—Asian J.* **2013**, *8*, 2828−2832.
(17) Wang, J. Y.; Yang, N. L.; Tang, H. J.; Dong, Z. H.; Jin, Q.; Yang, M.; Kisailus, D.; Zhao, H. J.; Tang, Z. Y.; Wang, D. Accurate Control of Multishelled Co_3O_4 Hollow Microspheres as High-Performance Anode Materials in Lithium-Ion Batteries. *Angew. Chem.* **2013**, *125*, 6545−6548.
(18) Hu, L.; Yan, N.; Chen, Q. W.; Zhang, P.; Zhong, H.; Zheng, X. R.; Li, Y.; Hu, X. Y. Fabrication Based on the Kirkendall Effect of Co_3O_4 Porous Nanocages with Extraordinarily High Capacity for Lithium Storage. *Chem.—Eur. J.* **2012**, *18*, 8971−8977.
(19) Alcántara, R.; Jaraba, M.; Lavela, P.; Tirado, J. L. $NiCo_2O_4$ Spinel: First Report on a Transition Metal Oxide for the Negative Electrode of Sodium-Ion Batteries. *Chem. Mater.* **2002**, *14*, 2847−2848.
(20) Sharma, Y.; Sharma, N.; Rao, G. V. S.; Chowdari, B. V. R. Lithium Recycling Behaviour of Nano-Phase-$CuCo_2O_4$ as Anode for Lithium-Ion Batteries. *J. Power Sources* **2007**, *173*, 495−501.
(21) Sharma, Y.; Sharma, N.; Rao, G. V. S.; Chowdari, B. V. R. Nanophase $ZnCo_2O_4$ as a High Performance Anode Material for Li-Ion Batteries. *Adv. Funct. Mater.* **2007**, *17*, 2855−2861.
(22) Li, J. F.; Xiong, S. L.; Li, X. W.; Qian, Y. T. A Facile Route to Synthesize Multiporous $MnCo_2O_4$ and $CoMn_2O_4$ Spinel Quasi-Hollow Spheres with Improved Lithium Storage Properties. *Nanoscale* **2013**, *5*, 2045−2054.
(23) Hu, L.; Zhang, P.; Zhong, H.; Zheng, X. R.; Yan, N.; Chen, Q. W. Foamlike Porous Spinel $MnxCo_{3-x}O_4$ Material Derived from $Mn_3[Co(CN)_6]_2{\cdot}nH_2O$ Nanocubes: A Highly Efficient Anode Material for Lithium Batteries. *Chem.—Eur. J.* **2012**, *18*, 15049−15055.
(24) Xing, Z.; Ju, Z. C.; Yang, J.; Xu, H. Y.; Qian, Y. T. One-Step Hydrothermal Synthesis of $ZnFe_2O_4$ Nano-Octahedrons as a High Capacity Anode Material for Li-ion Batteries. *Nano Res.* **2012**, *5*, 477−485.
(25) Liu, B.; Zhang, J.; Wang, X. F.; Chen, G.; Chen, D.; Zhou, C. W.; Shen, G. Z. Hierarchical Three-Dimensional $ZnCo_2O_4$ Nanowire Arrays/Carbon Cloth Anodes for a Novel Class of High-Performance Flexible Lithium-Ion Batteries. *Nano Lett.* **2012**, *12*, 3005−3011.
(26) Li, L. L.; Peng, S. J.; Cheah, Y. L.; Ko, Y.; Teh, P. F.; Wee, G.; Wong, C. L.; Srinivasan, M. Electrospun Hierarchical $CaCo_2O_4$ Nanofibers with Excellent Lithium Storage Properties. *Chem.—Eur. J.* **2013**, *19*, 14823−14830.
(27) Li, J. F.; Xiong, S. L.; Liu, Y. R.; Ju, Z. C.; Qian, Y. T. High Electrochemical Performance of Monodisperse $NiCo_2O_4$ Mesoporous Microspheres as an Anode Material for Li-Ion Batteries. *ACS Appl. Mater. Interfaces* **2013**, *5*, 981−988.
(28) Xiao, Y.; Hu, C. W.; Cao, M. H. Facile Microstructure Control of Mesoporous $Co_{1.29}Ni_{1.71}O_4$ and the Effect of the Microstructure on Lithium-Storage Performance. *Chem.—Eur. J.* **2013**, *19*, 10193−10200.
(29) Hu, L.; Zhong, H.; Zheng, X. R.; Huang, Y. M.; Zhang, P.; Chen, Q. W. $CoMn_2O_4$ Spinel Hierarchical Microspheres Assembled with Porous Nanosheets as Stable Anodes for Lithium-ion Batteries. *Sci. Rep.* **2012**, *2*, 986.
(30) Li, J. X.; Yang, M.; Wei, J. P.; Zhou, Z. Preparation and Electrochemical Performances of Doughnut-like $Ni(OH)_2$-$Co(OH)_2$ Composites as Pseudocapacitor Material. *Nanoscale* **2012**, *4*, 4498−4503.
(31) Mclntyre, N. S.; Cook, M. G. X-Ray Photoelectron Studies on Some Oxides and Hydroxides of Cobalt, Nickel, and Copper. *Anal. Chem.* **1975**, *47*, 2208−2213.
(32) Yuan, C. Z.; Li, J. Y.; Hou, L. R.; Zhang, X. G.; Shen, L. F.; (David) Lou, X. W. Ultrathin Mesoporous $NiCo_2O_4$ Nanosheets Supported on Ni Foam as Advanced Electrodes for Supercapacitors. *Adv. Funct. Mater.* **2012**, *22*, 4592−4597.
(33) Zhang, X.; Qian, Y. T.; Zhu, Y. C.; Tang, K. B. Synthesis of Mn_2O_3 Nanomaterials with Controllable Porosity and Thickness for Enhanced Lithium-Ion Batteries Performance. *Nanoscale* **2014**, *6*, 1725−1731.
(34) Xie, D.; Su, Q. M.; Dong, Z. M.; Zhang, J.; Du, G. H. L-Cysteine-Assisted Preparation of Porous NiO Hollow Microspheres with Enhanced Performance for Lithium Storage. *CrystEngComm.* **2013**, *15*, 8314−8319.
(35) Yan, N.; Hu, L.; Li, Y.; Wang, Y.; Zhong, H.; Hu, X. Y.; Kong, X. K.; Chen, Q. W. Co_3O_4 Nanocages for High-Performance Anode Material in Lithium-Ion Batteries. *J. Phys. Chem. C* **2012**, *116*, 7227−7235.
(36) Liang, C. C.; Cheng, D. F.; Ding, S. J.; Zhao, P. F.; Zhao, M. S.; Song, X. P.; Wang, F. The Structure Dependent Electrochemical Performance of Porous Co_3O_4 Nanoplates as Anode Materials for Lithium-Ion Batteries. *J. Power Sources* **2014**, *251*, 351−356.
(37) Su, D. W.; Kim, H. S.; Kim, W. S.; Wang, G. X. Mesoporous Nickel Oxide Nanowires: Hydrothermal Synthesis, Characterisation and Applications for Lithium-Ion Batteries and Supercapacitors with Superior Performance. *Chem.—Eur. J.* **2012**, *18*, 8224−8229.
(38) Han, F. D.; Bai, Y. J.; Liu, R.; Yao, B.; Qi, Y. X.; Lun, N.; Zhang, J. X. Template-Free Synthesis of Interconnected Hollow Carbon Nanospheres for High-Performance Anode Material in Lithium-Ion Batteries. *Adv. Energy Mater.* **2011**, *1*, 798−801.
(39) Mai, Y. J.; Shi, S. G.; Zhang, D.; Lu, Y.; Gu, C. D.; Tu, J. P. NiO-Graphene Hybrid as an Anode Material for Lithium Ion Batteries. *J. Power Sources* **2012**, *204*, 155−161.
(40) Xiong, S.; Chen, J.; Lou, X. W.; Zeng, H. Mesoporous Co_3O_4 and CoO@C Topotactically Transformed from Chrysanthemum-like $Co(CO_3)_{0.5}(OH){\cdot}0.11H_2O$ and Their Lithium-Storage Properties. *Adv. Funct. Mater.* **2012**, *22*, 861−871.
(41) Mei, W.; Huang, J.; Zhu, L.; Ye, Z.; Mai, Y.; Tu, J. Synthesis of Porous Rhombus-Shaped Co_3O_4 Nanorod Arrays Grown Directly on a Nickel Substrate with High Electrochemical Performance. *J. Mater. Chem.* **2012**, *22*, 9315−9321.
(42) Alcántara, R.; Jaraba, M.; Lavela, P.; Tirado, J. L. $NiCo_2O_4$ Spinel: First Report on a Transition Metal Oxide for the Negative Electrode of Sodium-Ion Batteries. *Chem. Mater.* **2002**, *14*, 2847−2848.
(43) Li, L. L.; Cheah, Y. L.; Ko, Y.; Teh, P.; Wee, G.; Wong, C. L.; Peng, S. J.; Srinivasan, M. The Facile Synthesis of Hierarchical Porous Flower-Like $NiCo_2O_4$ with Superior Lithium Storage Properties. *J. Mater. Chem. A* **2013**, *1*, 10935−10941.
(44) He, C. N.; Wu, S.; Zhao, N. Q.; Shi, C. S.; Liu, E. Z.; Li, J. J. Carbon-Encapsulated Fe_3O_4 Nanoparticles as a High-Rate Lithium Ion Battery Anode Material. *ACS Nano* **2013**, *7*, 4459−4469.
(45) Hu, L. L.; Qu, B. H.; Li, C. C.; Chen, Y. J.; Mei, L.; Lei, D. N.; Chen, L. B.; Li, Q. H.; Wang, T. H. Facile Synthesis of Uniform Mesoporous $ZnCo_2O_4$ Microspheres as a High-Performance Anode Material for Li-Ion Batteries. *J. Mater. Chem. A* **2013**, *1*, 5596−5602.
(46) Arico, A.; Bruce, P.; Scrosati, B.; Tarascon, J.; Schalkwijk, W. Nanostructured Materials for Advanced Energy Conversion and Storage Devices. *Nat. Mater.* **2005**, *4*, 366−377.
(47) Cai, J.; Li, Z.; Shen, P. Porous SnS Nanorods/Carbon Hybrid Materials as Highly Stable and High Capacity Anode for Li-Ion Batteries. *ACS Appl. Mater. Interfaces* **2012**, *4*, 4093−4098.
(48) Hu, L.; Chen, Q. W. Hollow/Porous Nanostructures Derived from Nanoscale Metal-Organic Frameworks Towards High Performance Anodes for Lithium-Ion Batteries. *Nanoscale* **2014**, *6*, 1236−1257.

(49) Ma, Y.; Zhang, C.; Jia, G.; Lee, J. Y. Nitrogen-Doped Carbon-Encapsulation of Fe_3O_4 for Increased Reversibility in Li^+ Storage by the Conversion Reaction. *J. Mater. Chem.* **2012**, *22*, 7845−7850.
(50) Song, R. R.; Song, H. H.; Zhou, J. S.; Chen, X. H.; Wu, B.; Yang, H. Y. Hierarchical Porous Carbon Nanosheets and Their Favorable High-Rate Performance in Lithium Ion Batteries. *J. Mater. Chem.* **2012**, *22*, 12369−12374.
(51) Sun, Y. M.; Hu, X. L.; Luo, W.; Huang, Y. H. Self-Assembled Hierarchical MoO_2/Graphene Nanoarchitectures and Their Application as a High-Performance Anode Material for Lithium-Ion Batteries. *ACS Nano* **2011**, *5*, 7100−7107.
(52) Han, F.; Li, D.; Li, W. C.; Lei, C.; Sun, Q.; Lu, A. H. Nanoengineered Polypyrrole-Coated Fe_2O_3@C Multifunctional Composites with an Improved Cycle Stability as Lithium-Ion Anodes. *Adv. Funct. Mater.* **2013**, *23*, 1692−1700.
(53) Luo, Y. S.; Luo, J. S.; Jiang, J.; Zhou, W. W.; Yang, H. P.; Qi, X. Y.; Zhang, H.; Fan, H. J.; Yu, D. Y. W.; Li, C. M.; Yu, T. Seed-Assisted Synthesis of Highly Ordered TiO_2@α-Fe_2O_3 Core/Shell Arrays on Carbon Textiles for Lithium-Ion Battery applications. *Energy Environ. Sci.* **2012**, *5*, 6559−6566.